Journal of Alloys and Compounds 722 (2017) 797–808

Contents lists available at ScienceDirect

Journal of Alloys and Compounds

journal homepage: http://www.elsevier.com/locate/jalcom

Characterization of Al-Si-Cu-Mg foams manufactured in-situ

I. Alfonso [a, *], I.A. Figueroa [b], L. Béjar [c], H.M. Gutiérrez [c], G. González [b], O. Hernández [d], C. Aguilar [e], G. Lara [b]

[a] Instituto de Investigaciones en Materiales, Unidad Morelia, Universidad Nacional Autónoma de México, Campus Morelia UNAM, Antigua Carretera a Pátzcuaro No. 8701, Col. Ex-Hacienda de San José de la Huerta, Morelia, Michoacán C.P. 58190, Mexico
[b] Instituto de Investigaciones en Materiales, Universidad Nacional Autónoma de México, Circuito Exterior SN, Ciudad Universitaria, Del, Coyoacán, Ciudad de Mexico. C.P. 04510, Mexico
[c] Facultad de Ingeniería Mecánica. Universidad Michoacana de San Nicolás de Hidalgo. Edificio W, Ciudad Universitaria. Morelia, Michoacán, C.P. 58000, Mexico
[d] Escuela Nacional de Estudios Superiores, Unidad Morelia, Universidad Nacional Autónoma de México, Campus Morelia UNAM, Antigua Carretera a Pátzcuaro No. 8701, Col. Ex-Hacienda de San José de la Huerta, Morelia, Michoacán, CP. 58190, Mexico
[e] Departamento de Ingeniería Metalúrgica y Materiales. Universidad Técnica Federico Santa María, Av. EspañaCasilla 110-V, Valparaíso, 1680, Chile

ARTICLE INFO

Article history:
Received 7 February 2017
Received in revised form
12 May 2017
Accepted 15 June 2017
Available online 17 June 2017

Keywords:
Microstructure
Metals and alloys
Foam
Heat treatment
Mechanical properties
Al-Si-Cu-Mg

ABSTRACT

This work presents the characterization of Al-6Si-3Cu-xMg (x = 7, 9 and 11 wt%) foams obtained through the in-situ process. Heat treatments which consisted on over-heating the alloys during 6 h at 520, 560 and 600 °C were performed. The microstructural changes, the quantification and measurement of sizes and shapes of second phases and pores were carried out by means of Optical Microscopy (OM), X-Ray Diffraction (XRD) and Scanning Electron Microscopy (SEM). Compression tests and density measurements were also assessed. The results showed porosities ranging from 2 to 40%, with pore sizes from 20 to 150 μm, shape factors from 0.59 to 0.72, and maxima relative densities between 0.89 and 0.91. The formation of these pores was attributed to the dissolution and melting processes of the second phases and the shrinkage originated after their solidification. Fragmentation, spheroidization and coarsening of second phases during the solution heat treatment was also observed. It was found that the microstructures of the foams, including pores and second phases, strongly depended on the over-solution temperature and the Mg content. Temperature was the manufacturing variable that most affected the size and quantity of the pores produced.

1. Introduction

Day to day new advanced materials are studied for different applications. One of these materials are the metallic foams, whose importance has increased due to their exceptional mechanical, thermal, acoustic, electrical and chemical properties derived from their structures [1–3]. The most important methods for manufacturing metallic foams include infiltration of liquid metal, powder metallurgy and liquid processes bubbling gas through molten metal or adding foaming agents [3,4]. These manufacturing processes are classified according to the state of matter in which the metal is processed. A previous work [5] showed the initial results about a new solid state method for producing foams without foaming agents or space holders for quaternary Al-Si-Cu-Mg alloys, using heat treatments at temperatures higher than the melting point of second phases. With the mentioned solid state method Al-Cu-Fe foams with porosities above 60% were also produced [6]. This method has been only used for these two Al alloys, where the formation of the pores is attributed to the shrinkage generated by localized peritectic reactions after melting of specific second phases. In the case of the Al-Si-Cu-Mg alloys, the reported second phases were the eutectic Al-Si, Q ($Al_5Mg_8Cu_2Si_6$), Al_2Cu and Mg_2Si, in addition to other complex intermetallic compounds [7]. Although for these alloys the Mg content generally remains low (approximately 0.5 wt%), previous works have studied much higher Mg contents, between 0.5 and 7.0 wt% [8], and recently up to 11% [5]. The effect of this element is very important, as it leads to significant modifications on the microstructure, mainly forming Mg_2Si and modifying Cu-rich phases from Al_2Cu to Q ($Al_5Mg_8Cu_2Si_6$) [5,8]. Before our previous works about manufacturing metallic foams

* Corresponding author.
E-mail address: ialfonso@unam.mx (I. Alfonso).

http://dx.doi.org/10.1016/j.jallcom.2017.06.173
0925-8388/

using over-heat treatments [5,6], all the reported works tried to avoid pores formation due to the localized melting of second phases, being the optimal (and maximum) reported solution temperature close to 500 °C [9–11]. The heat treatment conditions tend to control the resulting microstructure, such as the aspect ratio of the particles, their sizes, and the spacing between them, essential parameters for obtaining high ductility [12]. These changes are originated by fragmentation, spheroidization and coarsening of the phases. To date, these modifications were only analyzed for second phases. Nevertheless, since the applications of these alloys have been widespread, it is also very important to analyze the modifications related to the induced porosity. Therefore, the objective of the present work is to obtain a detailed characterization of metallic foams manufactured in-situ through over-solution heat treatments performed on Al-6Si-3Cu-xMg alloys with Mg contents of 7, 9 and 11 wt%. The effect of the solution temperature and the Mg content on the microstructure, including induced porosity and second phases will be also analyzed.

2. Experimental details

Three experimental Al-Si-Cu-xMg alloys were obtained using Al, Si, Cu and Mg of high purity (>99.95%). Table 1 shows the resulting chemical compositions, modifying the Mg content beyond the reported in literature [7,8]. This with the aim of producing significant microstructural modifications, i.e. higher amount of secondary phases. The melting and casting of the alloys were carried out using graphite crucibles in a Leybold-Heraeus induction furnace with a controlled Ar atmosphere. The molten alloys were poured into cylindrical molds to obtained bars of 15 cm in height and 2 cm in diameter.

The as-cast alloys were sectioned in cylindrical samples (1.0 cm in height), polished using standard metallographic techniques and characterized by OM and SEM, using respectively a Nikon EPIPHOT 300 optical microscope, and a JEOL JSM 7600F scanning electron microscope operated at 20 kV, with a BRUKER XFlash6130 energy dispersive X-ray spectrometer (EDX) attached. The alloys were also analyzed by X-ray diffraction (XRD), using a Siemens 400 X-ray diffractometer, with CuKα radiation at 30 kV and 25 mA; and by differential thermal analysis (DTA) in order to determine the phase transition temperatures of the different phases, which are related to the formation of the porosity due to the localized melting or solid state reactions [6]. This study was performed between 200 and 800 °C with a heating rate of 10 °C/min, using a TA Instruments SDT Q-600 calorimeter.

The alloys were then solution heat treated during 6 h at 520 °C, 560 °C and 600 °C (temperatures determined according DTA results) in a forced-air furnace. Next, the samples were air cooled, polished, and examined using OM and SEM to observe microstructural changes in the secondary phases and in the induced porosity. The microstructures captured in the images were analyzed through the pixel's intensity using ImageJ software [13]. As first step, the obtained gray level images were transformed to binary images. Second phases are clearly distinguished from the matrix, and can be simply discriminated by their different gray-contrast. An effective segmentation method used to analyze the second phases in these images is the global thresholding method, described by Liu et al. [14]. There, the gray-level image is converted into a binary image by selecting an appropriate gray-level threshold in order to separate second phases from the background (α–Al). The method used is based on a gray scale value comparison, using a reference sample (only α-Al) and adjusting the threshold level to a certain gray scale value.

Table 1
Chemical composition (in wt%) of the experimental alloys.

Alloy	Si	Cu	Mg	Fe	Mn	Zn	Al
A07	6.05	3.12	7.02	0.02	0.01	0.01	Balance
A09	6.10	2.93	9.08	0.01	0.01	0.01	Balance
A11	5.94	3.09	10.89	0.01	0.01	0.01	Balance

Heat treated samples were also studied using XRD in order to analyze the phase transformations. For the study of the compressive behavior of the obtained materials, compression tests of the as-cast alloys and the foams were conducted on an Instron 1125–5500R materials testing machine with a crosshead speed of 0.1 mm/min, according to the ASTM E9-09, "Standard Test Methods of Compression Testing of Metallic Materials at Room Temperature", using cylindrical samples of 12 mm diameter and 10 mm in length. The densities of the materials were determined at room temperature by the flotation method using ethanol in a Sartorius Quintix 124-1s analytical balance. Density measurements were repeated three times at the given conditions.

Besides the characterization of the porosity, the evolution of the morphology of secondary phases is a very important characteristic to be determined, due to the above-mentioned decomposition, fragmentation, spheroidization and coarsening of such phases. Thus, the sizes of second phases and pores were determined through the equivalent diameter (D_e), defined as the diameter of a circle with equivalent area, and given by Equation (1), where A_p is the particle area and n the number of features measured [12]:

$$D_e = \frac{1}{n}\sum_{i=1}^{n}\left(\frac{4A_{pi}}{\pi}\right)^{1/2} \quad (1)$$

Shape factors (F) were also determined [12] in order to analyze not only the transformation of the second phases after heat treatment but also the shape of the pores. F is a dimensionless parameter defined in Equation (2), where P_p is the perimeter. A perfect circle will have a shape factor of 1, while the shape factor of a line will approach to zero.

$$F = \frac{1}{n}\sum_{i=1}^{n}\left(\frac{4\pi A_{pi}}{P_{pi}^2}\right) \quad (2)$$

3. Results and discussion

3.1. Analysis of the as-cast alloys

Fig. 1 a–c shows OM micrographs of the as-cast microstructures for the experimentally obtained alloys. This technique was enough to identify the phases with different gray levels, recognized in the microstructures. It is important to note the significant microstructural modifications originated as Mg content increases. For the alloy A07 (Fig. 1a) it can be observed the presence of four well known second phases i.e. the eutectic Al-Si, Chinese script eutectic Mg_2Si, Al_2Cu and $Al_5Mg_8Cu_2Si_6$ (Q phase). It is observed that the Al_2Cu phase is slightly lighter when compared to Q, while Mg_2Si is easy to differentiate due to its dark contrast. For the alloy A09, the microstructure showed a significant presence of primary Mg_2Si particles besides the eutectic Al-Mg_2Si (Fig. 1b). The size of the Cu-rich phases (Al_2Cu + Q) increased, while the quantity of Al-Si eutectic decreased. For the alloy A11 (Fig. 1c) it is observed that the size of Cu-rich phases is higher than that for the alloys with lower Mg content. It was also observed a higher content of eutectic Al-Si, while eutectic Mg_2Si mainly appears again as Chinese script (although few primary particles were observed). The presence of

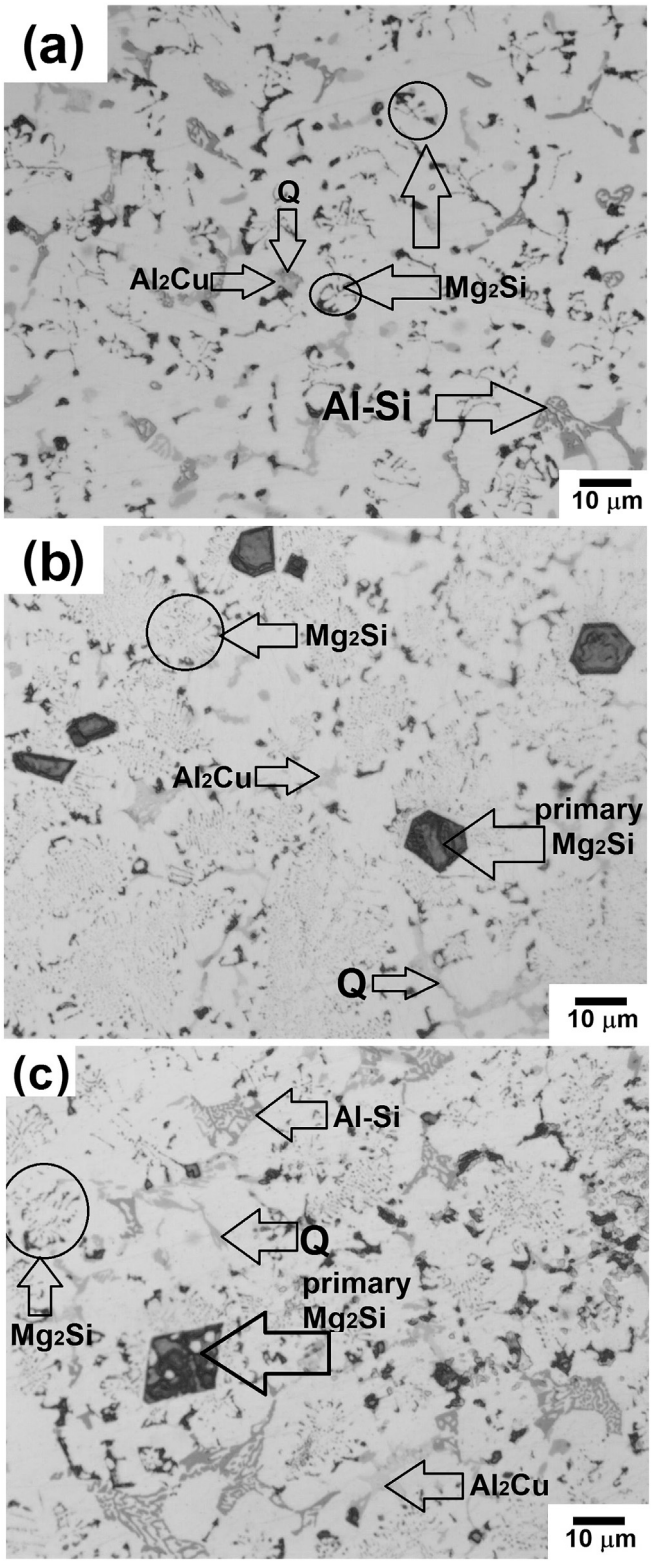

Fig. 1. Optical micrographs of the as-cast alloys for Mg contents of: (a) 7%, (b) 9%, and (c) 11%. Arrows indicate second phases.

these phases agrees well with works found in literature for different Al alloys [15–19]. EDX analysis did help to identify these phases, however, the XRD analysis corroborated this assumption, as will be presented.

The above mentioned microstructural modifications are summarized in Table 2. There, it was observed that the total volume of second phases increased slightly as a function of the Mg content. Then, a first condition for using over-solution heat treatment as foams manufacturing method (to obtain a maximum amount of second phases) is achieved. Nevertheless, the analysis of second phases also revealed that the increase in the Mg content does not led to a constant increment in the amount of each phase. This result could be attributed to the formation of the primary Mg_2Si particles, as this phase is the first that solidifies. Due to its role on the porosity formation, a further analysis of this phase will be carried out and reported elsewhere.

Fig. 2 shows the XRD patterns obtained from the as-cast alloys. The most intense peaks, besides the α-Al matrix, correspond to the phases already observed in Fig. 1a–c: i.e. Si (eutectic Al-Si), Mg_2Si, Al_2Cu and $Al_5Mg_8Cu_2Si_6$ (Q phase), corroborating the results obtained from the micrographs and EDX analyses. The intensity of the peaks of Si and Q was smaller for the A09 alloy when compared to those of the A07 alloy, however, for the alloy A11 the intensity for both phases did increase considerably. Contrary to this result, Mg_2Si and Al_2Cu peaks intensity increased for the alloy with 9% Mg, and decreased for the alloy A11. The formation of Mg_2Si (mainly primary particles, which is the "second phase" that first precipitates during the solidification process, at temperatures between 657 and 599 °C [17]) leads to a decrease of Mg and Si concentration in the remaining liquid phase for the alloy A09, favoring the precipitation of Al_2Cu and reducing the final quantity of Q and eutectic Al-Si. These results agreed well with those observed in the microstructures shown in Fig. 1a–c and Table 2.

Fig. 3a–c shows the DTA curves of the as-cast alloys heating from 200 to 800 °C. Three endothermic peaks can be observed, these represents the dissolution or melting events of the phases. This analysis was mainly carried out for determining the temperatures for the over-solution heat treatments and will be further used as starting point for in-situ studies of the secondary phases transformation. The first endothermic peaks are barely observable, and changed according to the chemical composition of the alloys: 508, 509 and 506 °C for the alloys A07, A09 and A11, respectively. These peaks are similar to those reported by Lasa and Rodriguez-Ibabe, showing a melting event at temperatures between 507 and 511 °C for an Al–12Si–4.4Cu–1.3 Mg alloy [20]. This was also observed in the thermal analysis reports of other similar alloys [11,15,17]. These works attributed this endothermic effect to the reaction of α-Al + Al-Si + Al_2Cu + $Al_5Mg_8Cu_2Si_6$ solid phases to form a liquid phase. The small quantity of Al-Si eutectic for the experimentally produced alloys could cause these barely observable peaks, taking into account that the magnitude of these incipient melting effects increases when increasing the amount of intermetallic phases. The second endothermic peaks, at approximately 540 °C (541, 538 and 542 °C for the alloys A07, A09 and A11, respectively), could correspond to the reaction: α-Al + Al-Mg_2Si + Al_2Cu + $Al_5Mg_8Cu_2Si_6$ = liquid. According to the work of Farahany et al. [17], in the Al–13 Mg–7Si–2Cu alloy an extensive melting of Al_2Cu + $Al_5Mg_8Cu_2Si_6$ occurs at a temperature below 546 °C. The last endothermic peaks of the DTA curve, approximately at 585 °C (585, 588 and 581 °C for the alloys A07, A09 and A11, respectively), could be associated to the melting of the eutectic Al-Mg_2Si. This also agrees with the results of reference [17], where it was reported that this transformation occurs at a temperature between 577 and 599 °C through the reaction α-Al + Al-Mg_2Si = liquid. It will be possible to analyze these asseverations by means of the SEM images and XRD analysis. It is important to mention that the temperatures for the over-solution heat treatments must be slightly higher than those of the endothermic peaks. Therefore, 520, 560 and 600 °C were selected in order to induce

Table 2
Volume % of second phases for the experimental alloys.

Alloy/Phase	Mg_2Si	Primary Mg_2Si	Al_2Cu	Q	Al-Si eutectic	Total
A07	3.65 ± 1.02	0	1.52 ± 0.09	3.56 ± 0.69	3.80 ± 0.88	12.53 ± 2.51
A09	5.01 ± 1.03	4.90 ± 0.88	1.67 ± 0.33	2.89 ± 0.52	1.27 ± 0.03	15.68 ± 3.10
A11	4.50 ± 1.00	1.01 ± 0.08	0.97 ± 0.05	5.29 ± 0.72	5.33 ± 1.11	16.73 ± 3.61

porosity formation.

3.2. Analysis of the over-heat treated alloys

3.2.1. Porosity

For the analyses of the porosity and the second phases, OM images are shown in Fig. 4a–c to 6a-c. Fig. 4a–c shows, for the alloy with 7% of Mg, the porosity induced by heat treatments at temperatures higher than those related to the peaks observed in Fig. 3a. As can be observed, important porosities were induced in all cases. Fig. 4a shows the case of an over-heat treatment at 520 °C for 6 h, presenting pores with an average equivalent diameter of 20 ± 3 μm, shape factor of 0.62 and a porosity of 4.2%. Second phases are barely visible at this magnification. Fig. 4b shows the case of an over-heat treatment at 560 °C for 6 h, presenting pores with an average equivalent diameter of 58 ± 9 μm, shape factor of 0.72 and a porosity of 18%. It is important to remark the significant increment in the porosity and pore size for this temperature. Second phases also increased their sizes and will be further quantified. Fig. 4c shows the alloy heat treated at 600 °C during 6 h. For this case, the resulting porosity was 31%, with an average equivalent pore diameter of 115 ± 25 μm, and a shape factor of 0.60. Second phases with spherical geometry are clearly observed in this image.

Fig. 5a–c shows, for the alloy with 9% of Mg, the porosity induced by heat treatments at temperatures higher than those observed for the peaks in Fig. 3b. The behavior is similar to the detected for the alloy A07. Fig. 5a shows the case of an over-heat treatment of 520 °C during 6 h, presenting pores with an average equivalent diameter of 22 ± 3 μm, shape factor of 0.59 and a porosity of 3.3%. Fig. 5b shows the case of an over-heat treatment of 560 °C during 6 h, presenting pores with an average equivalent diameter of 33 ± 7 μm, shape factor of 0.69 and a porosity of 8.6%. At 520 and 560 °C, second phases of two sizes are, now, easily observed i.e. i) small size particles, presumably eutectic Mg_2Si and Cu-rich phases; and ii) bigger particles, presumably primary Mg_2Si particles observed in the as-cast condition. This asseveration will be further analyzed. Finally, Fig. 5c shows the alloy heat treated at 600 °C during 6 h. For this case, the size of the individual pores was 95 ± 16 μm, with a porosity of 25.3% and a shape factor of 0.61. Second phases also increased their size for this condition, as for the alloy A07. As can be observed, for this alloy the increase in pore size and porosity % was less significant than for the alloy A07. A plausible explanation for this behavior could be the already mentioned presence of primary Mg_2Si particles. This phase is difficult to dissolve and is reported that it melts down at a temperature higher than the one used in this work [17]. This fact decreases the amount of melted phases, which are needed for the transformation and further pore formation.

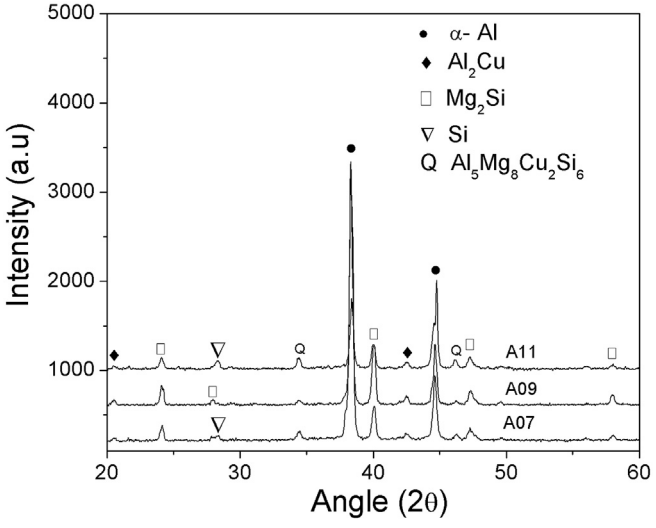

Fig. 2. XRD patterns for the experimental alloys.

Fig. 6a–c shows, for the alloy with 11% of Mg, the porosity induced by heat treatments at temperatures with the aforementioned conditions. The behavior of the porosity was similar to the observed for the alloys A07 and A09. Fig. 6a shows the case of an over-heat treatment of 520 °C during 6 h, presenting pores with an average equivalent diameter of 20 ± 3 μm, shape factor of 0.63 and a porosity of 1.9%. Fig. 6b shows the case of an over-heat treatment at 560 °C for 6 h, presenting pores with an average equivalent diameter of 35 ± 6 μm, shape factor of 0.68 and a porosity of 6%. At temperatures of 520 and 560 °C, second phases of two sizes were also easily observed. Finally, Fig. 6c shows the alloy heat treated at 600 °C for 6 h. The size of the individual pores was 150 ± 20 μm, with a shape factor of 0.63 and a porosity of 40%. Second phases also increased their size for this condition, similar to the alloys with lower Mg content, heat treated at 600 °C.

The information obtained about the induced porosity can be observed in Fig. 7a–c. The highest porosities (Fig. 7a) and the biggest pores (Fig. 7b) were obtained for the alloys heat treated at 600 °C, while the maxima shape factors (the more rounded pores, Fig. 7c) were obtained for the alloys heat treated at 560 °C. The effect of the Mg content was also very important, but always depending on temperature, being the maximum porosity for the alloys with the highest content of this element heat treated at 600 °C.

The statistical analysis (using Pareto's diagrams and ANOVA) of these results allowed correlating the manufacturing parameters to the physical characteristics of the porosity. It was possible to determine that heat treatment temperature was the parameter that most influenced both, porosity percentage and pore size. Otherwise, it was observed that the amount of Mg content did not affect the porosity percentage and pore size, however, it was a strong influence on the morphology of the Mg_2Si phase. The significant presence of this phase as primary particles for the alloy with 9% Mg dropped the amount of melted phases, a required condition for phase transformation and pore formation. Equation (3) and Table 3 show the correlation equations obtained after the analyses of porosity percentage (ϕ) and equivalent diameter (D_e). The high values for R^2 demonstrate the good representation by the assumed relationships. Correlation equation obtained for shape factor was more complicated and presented a low R^2 correlation (0.63).

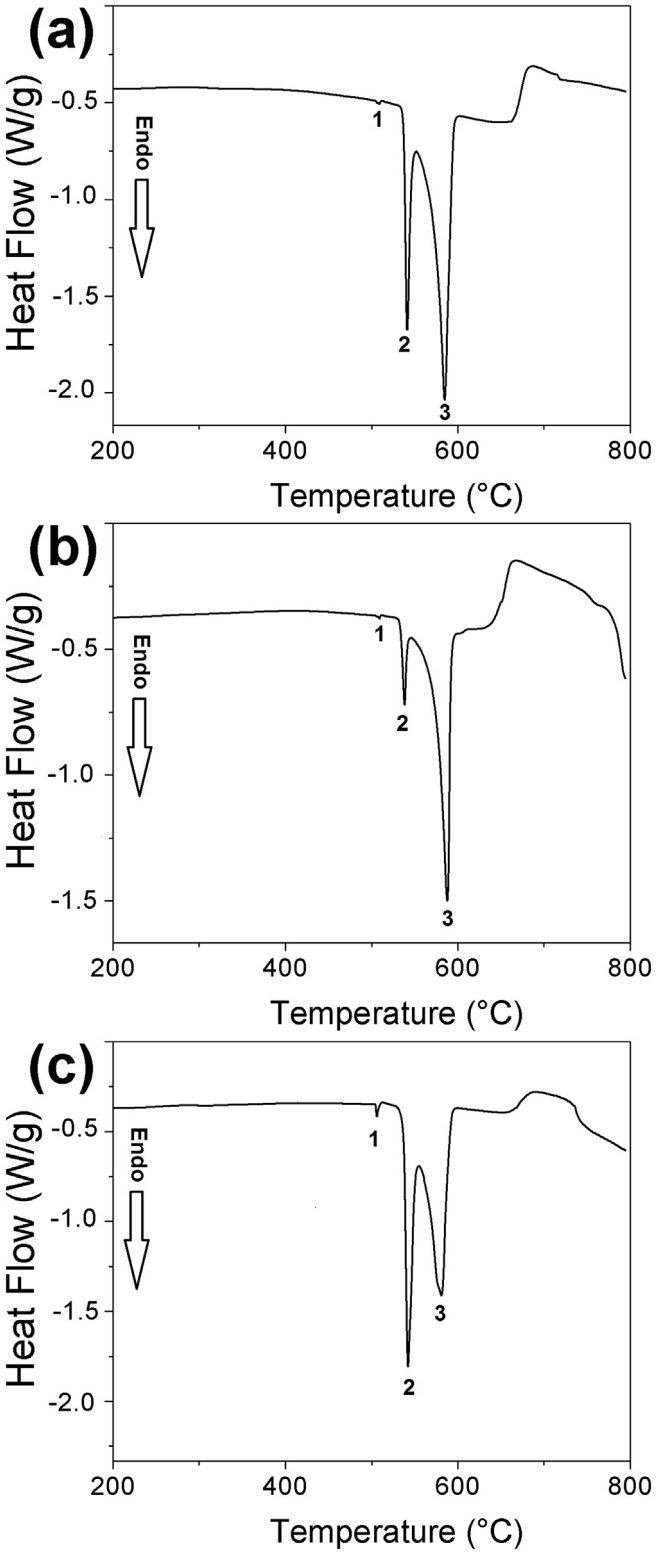

Fig. 3. DTA curves showing the transformation temperatures of the phases for the as-cast alloys: (a) A07, (b) A09, and (c) A11.

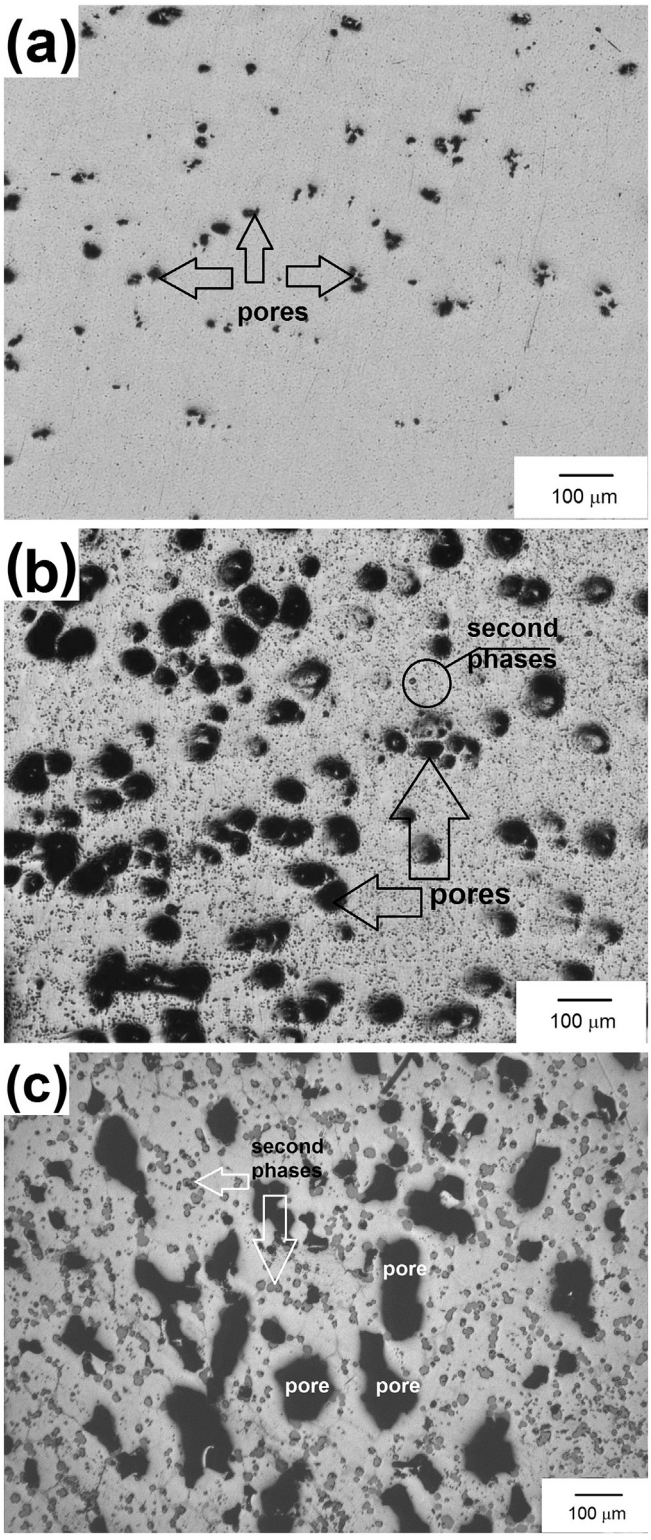

Fig. 4. Optical micrographs showing the porosity originated in the alloy with 7% Mg over-solution heat treated during 6 h at: (a) 520 °C, (b) 560 °C, and (c) 600 °C.

$$y_i = (\beta_0 + \beta_1 T + \beta_2 Mg)^{\frac{1}{\lambda}} \quad (3)$$

where y_i can be ϕ or D_e, while β_0, β_1, β_2 and λ are defined according to Table 3.

The presence of pores promoted important changes in the densities of the investigated materials. For the as-cast A07, A09 and A11 alloys, these values were 2.49, 2.58 and 2.43 g/cm^3, respectively; while for the materials heat treated at 600 °C the densities were 2.23, 2.36 and 2.21 g/cm^3. Then, the relative densities (defined

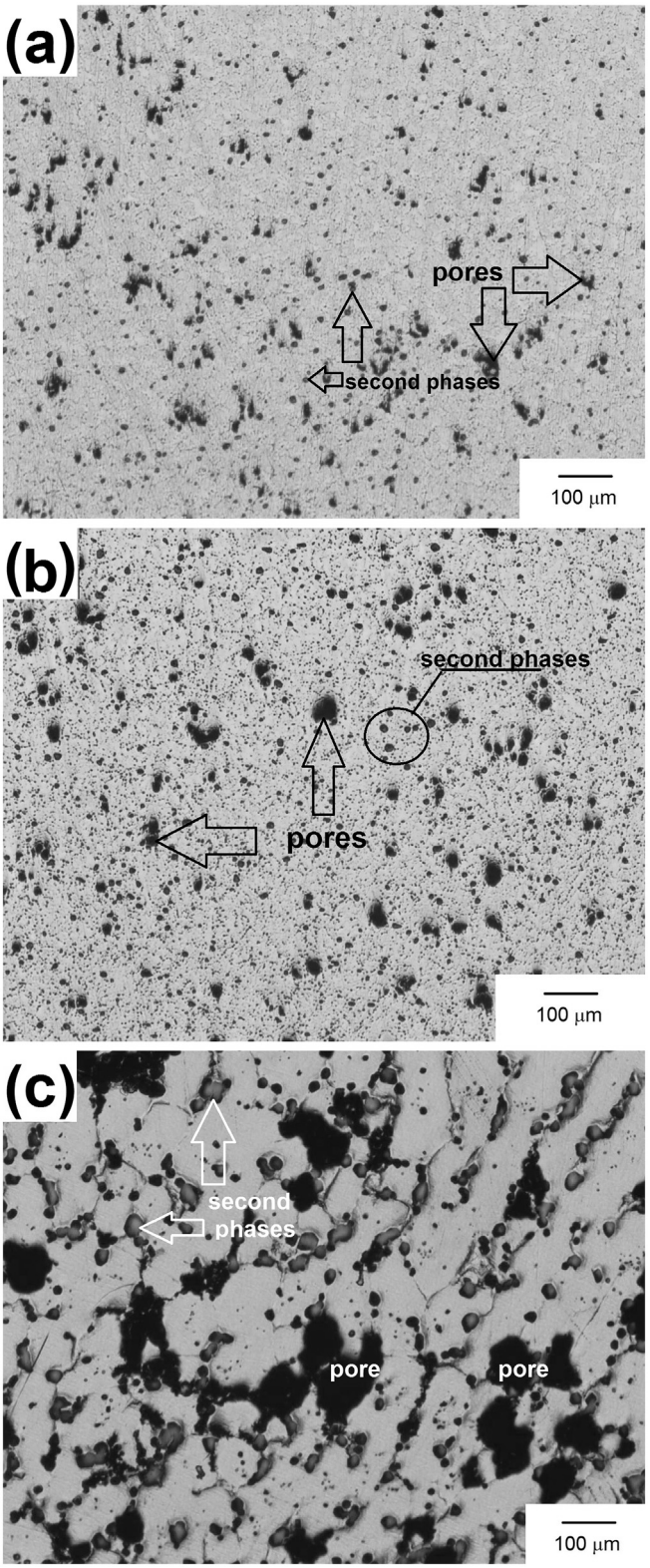

Fig. 5. Optical micrographs showing the porosity originated in the alloy with 9% Mg over-solution heat treated during 6 h at: (a) 520 °C, (b) 560 °C, and (c) 600 °C.

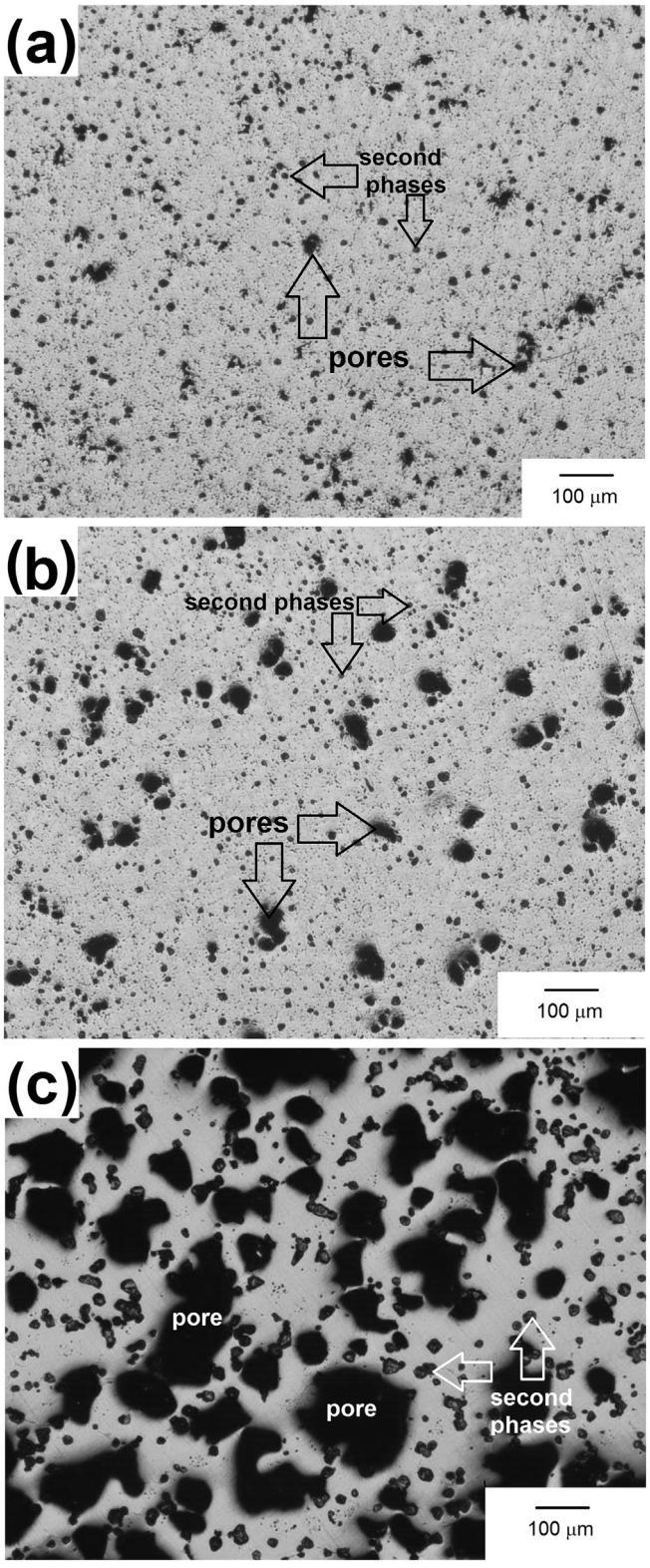

Fig. 6. Optical micrographs showing the porosity originated in the alloy with 11% Mg over-solution heat treated during 6 h at: (a) 520 °C, (b) 560 °C, and (c) 600 °C.

as the ratio between the density of the foams and the density of the metal matrix) reached values of 0.89, 0.91 and 0.91, respectively. These values are not as high as the observed for metallic foams obtained using other methods such as powder metallurgy or infiltration using space holders. Nevertheless, the porosity obtained in the present work is important due to the contribution that could present in order to increase total porosity of the foams. According to the already mentioned statistical analyses, in order to obtain

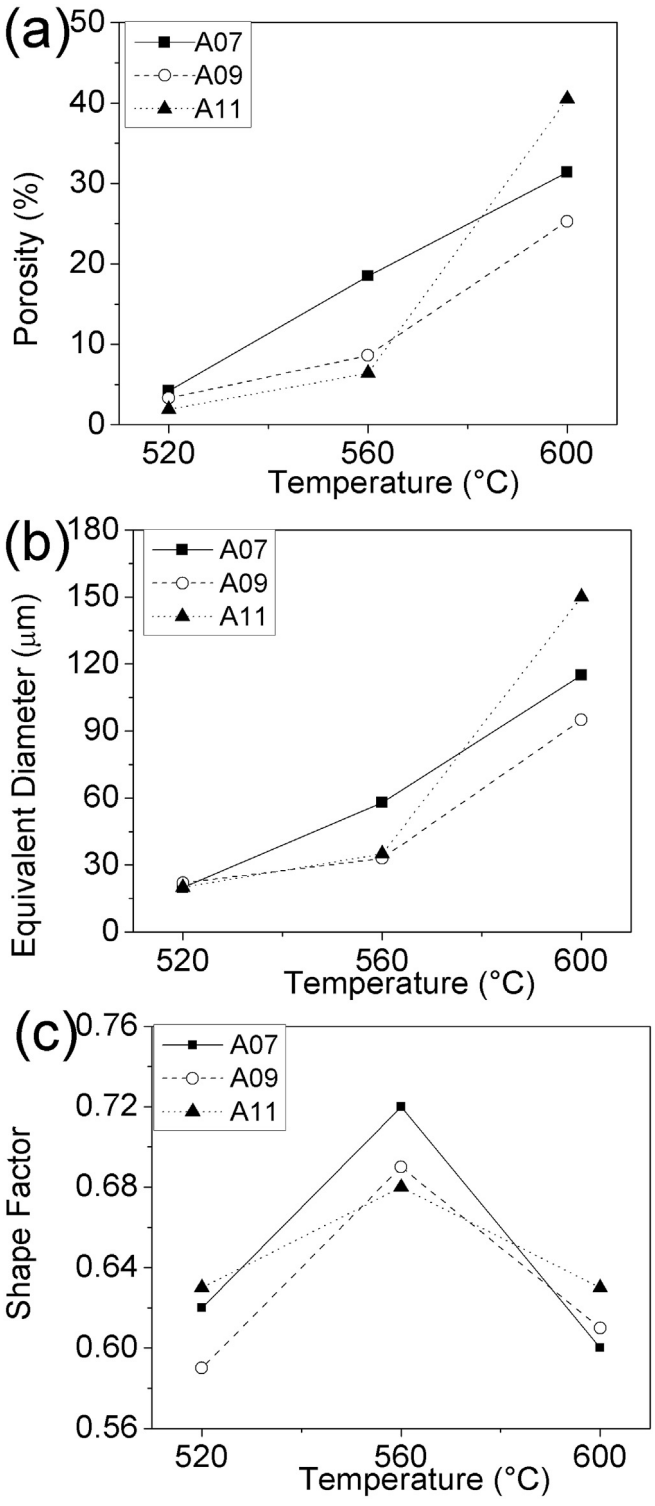

Fig. 7. Porosity percentages (a), equivalent diameters (b), and shape factors (c) of the pores induced in the experimental alloys using different over-solution heat treatments.

Table 3
Values for regression Equation (3) for porosity (ϕ) and equivalent diameter (D_e).

y_i/values	β_0	β_1	β_2	λ	R^2
ϕ	1.238	-5.391×10^{-4}	2.449×10^{-3}	−0.019	0.91
D_e	0.829	−0.001	0.002	−0.6	0.93

high porosities (percentage and size of pores) the over-solution heat treatment must be conducted at the highest possible temperature. The effect of Mg content on density was not significant, mainly due to the fact that this element not only has effect on the porosity but also on the final microstructure of the treated alloys, and presents an intrinsic contribution to final density.

3.2.2. Second phases

For a better analysis of the second phases present after the over-solution heat treatments, the alloys were characterized using SEM (backscattered electrons, BSE). Fig. 8a–c shows images of the evolution of the second phases for the alloy A07 heat treated during 6 h at different temperatures. When comparing to the microstructure of the as-cast alloy (already analyzed in Fig. 1a), important modifications occurred for the three temperatures. For specimens treated at 520 °C (Fig. 8a) second phases are already fragmented in small rounded particles, a process reported in literature for conventional heat treatments in Al alloys [8,12]. Fragmentation (disintegration of second phase structures in small particles) occurred for both, the eutectic Mg_2Si and Q (EDX for Q in Fig. 8d), being respectively their equivalent diameters 3.49 and 5.11 μm, while the shape factors were 0.65 and 0.52. The Al_2Cu and Si phases were not observed for this sample. For the specimen treated at 560 °C (Fig. 8b) it can be also observed the spheroidization and coarsening of Mg_2Si and Q (Al_2Cu and Si were not observed). When compared to the alloys treated at 520 °C, these phases increased in both, the equivalent diameters (now 7.23 μm for Mg_2Si and 7.89 μm for Q), and the shape factors (now 0.73 for Mg_2Si and 0.61 for Q). Otherwise, for the specimen treated at 600 °C (Fig. 8c) there were two important changes: A) the Mg_2Si phase is present as primary phase particles instead of eutectic Mg_2Si (see EDX in Fig. 8e, where the big size for primary particles allows to obtain a characteristic EDX with low intensity Al peaks; and EDX in Fig. 8f, characteristic for eutectics, with most intense Al peaks). These primary particles are significantly bigger than the eutectic ones, reaching a maximum average size of 18.11 μm. Note that the magnification for Fig. 8c was different (1000x for Fig. 8a and b, 500x for Fig. 8c). B) The second important change was that Cu-rich phases are mainly present as Al_2Cu (see EDX in Fig. 8g) instead of the Q phase. Nevertheless, for this alloy some small Q particles were still observed (approximately 3 μm), as can be seen in Fig. 8h. These results agreed with those observed using XRD.

Similar behavior was observed after over-heat treating for the alloys A09 and A11, except for the primary Mg_2Si particles already observed since the as-cast conditions, with no modifications due to their low solubility and high melting temperature. In order to analyze the above-mentioned process for all the alloys, including fragmentation, spheroidization and coarsening of second phases, Fig. 9a–b shows the behavior of equivalent diameters (D_e) and shape factors (F), for eutectic Mg_2Si and Q. As can be observed, equivalent diameters increased as a function of the temperature, being always higher for Q (Fig. 9a). Otherwise, the shape factors also increased as the temperature increases, being always higher for eutectic Mg_2Si than for Q (Fig. 9b). These results show the spheroidization and coarsening processes, and demonstrate that Q phase is more difficult to dissolve than eutectic Mg_2Si, which agrees with the literature [8]. The data for 600 °C are not presented in this work, due to the fact that for this temperature the phases are different and cannot be compared to the previously analyzed ones. Besides the Al_2Cu phase has not a rounded shape but block-like, as previously observed in Fig. 8c.

The obtained materials were analyzed using XRD in order to corroborate the microstructural modifications observed by means of OM and SEM. Fig. 10a–c shows the XRD patterns for the alloys heat-treated at different temperatures. At 520 °C, for all the alloys,

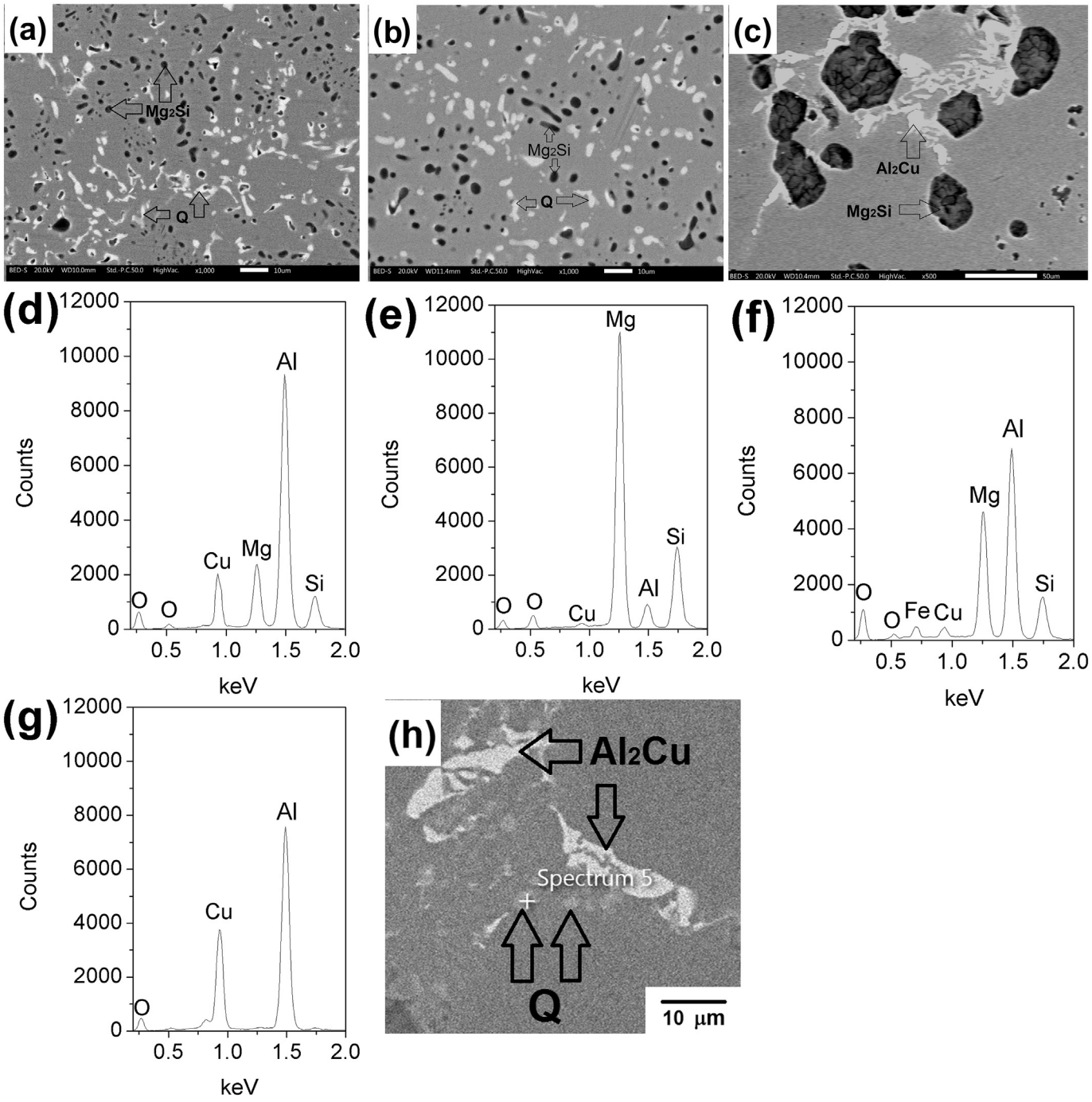

Fig. 8. SEM-BSE micrographs showing the second phases evolution and the porosity originated in the alloy with 7% Mg over-solution heat treated during 6 h at temperatures of: (a) 520 °C, (b) 560 °C, and (c) 600 °C; and EDX of the phases Q (d), primary Mg_2Si (e), eutectic Mg_2Si (f) and Al_2Cu (g). Q particles remaining after a heat treatment at 600 °C can be observed, although the dominant phase is Al_2Cu (h).

the most important modification in the diffraction patterns was the absence of the Al-Si eutectic and Al_2Cu peaks. This result agreed with the observed using SEM, where these phases were not observed. This could be attributed to their dissolution or incipient melting because they are much easier to dissolve than Q phase. At 560 °C the most important change occurred for Q and Mg_2Si, the intensity of their peaks dropped, when compared to those treated at 520 °C. This behavior could be attributed to their dissolution or incipient melting, agreeing well with the SEM results, here, no new phases were observed at this temperature, only spheroidization and coarsening was detected. Nevertheless, it is important to analyze in detail this microstructure due to the possible melting and transformation of Q phase [17]. Otherwise, for 600 °C the intensity of Al_2Cu, Si and Mg_2Si peaks increased significantly, decreasing the intensity for the Q phase peaks, corroborating the transformation of Q into Al_2Cu.

In order to analyze the phase transformations, reduced time heat treatments (5 min) at 520, 560 and 600 °C were conducted on polished alloy samples. The surfaces of the heat-treated alloys were observed using SEM in order to analyze the microstructural

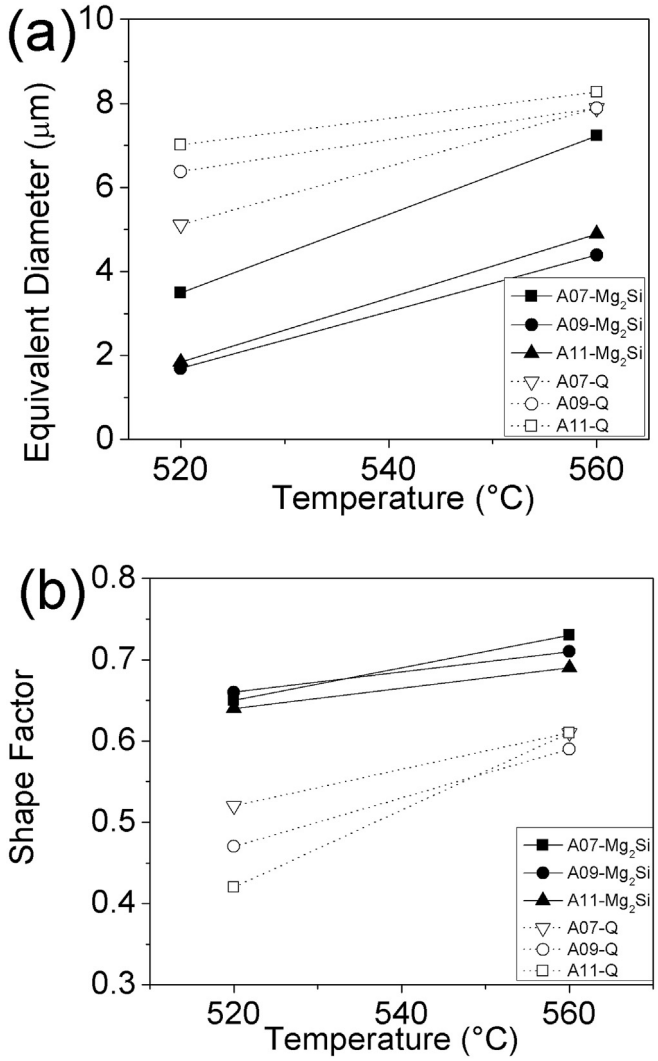

Fig. 9. Equivalent diameters (a), and shape factors (b) of the second phases for the alloys over-solution heat treated at 520 and 560 °C for 6 h.

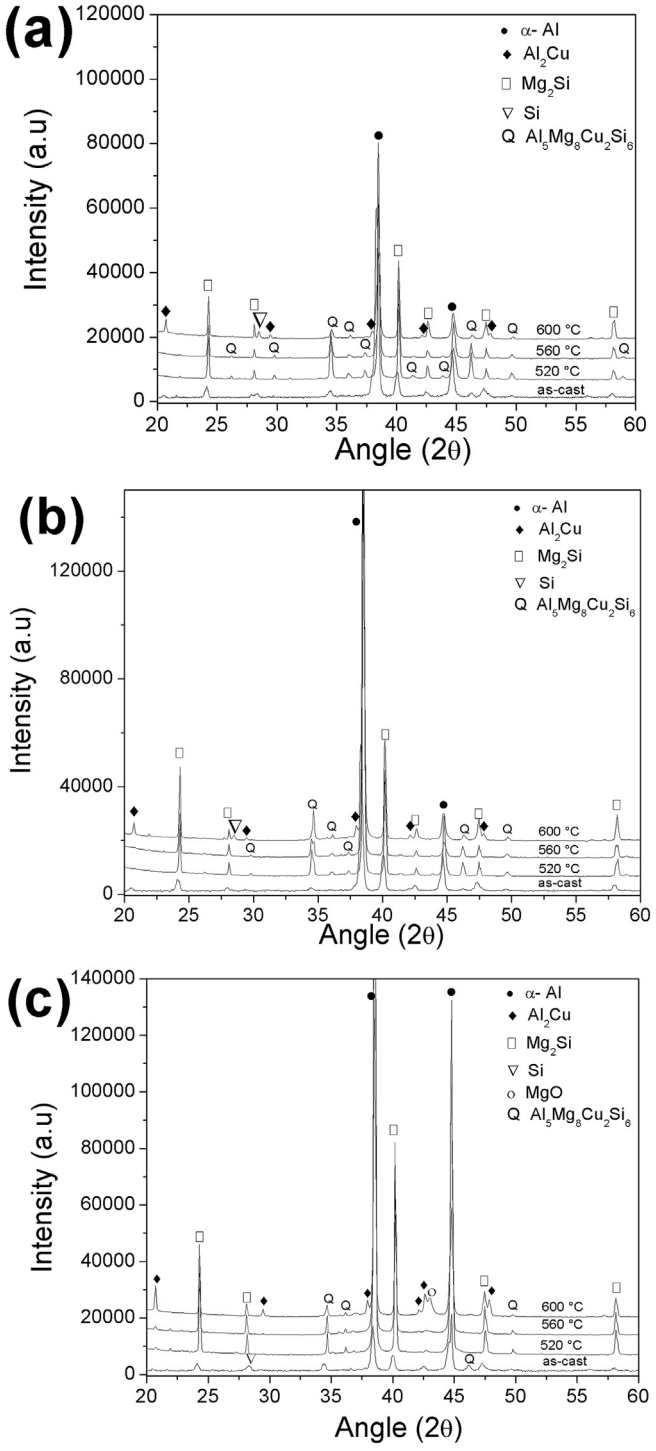

Fig. 10. XRD patterns for the alloys with 7% Mg (a), 9% Mg (b), and 11% Mg (c) over-solution heat treated during 6 h at temperatures of 520 °C, 560 °C and 600 °C.

modifications. The alloy A11 was selected as study case. For a heat treatment at 520 °C, it was not observed the presence of Al_2Cu and eutectic Si (see Fig. 11a); and Mg_2Si was already observed as rounded particles instead of Chinese script showing that fragmentation and spheroidization occur even at very short times. On the other hand, spheroidization of the Q phase is not observed yet; and its quantity clearly decreased, being located around the Mg_2Si phase. Otherwise, dendrites forming splitting patterns can be observed (circled in Fig. 11a). The EDX studies of these dendrites showed that their chemical compositions are enriched with all the alloying elements, suggesting that they could be composed by elements from Cu-rich phases and Si, agreeing with the observed by the DTA studies (Fig. 3 a–c, peaks n. 1). This result suggests that the melted material moved from Mg_2Si - Cu-rich phases interface to the α-Al matrix, transforming into the Q phase. This could explain the presence of Q instead of Al_2Cu and eutectic Si for a heat treatment of 6 h, already observed by XRD and SEM. It is thought that the solidification shrinkage of these melts tends to form the highly porous structure. At 560 °C, the characteristics of the processes observed at 520 °C are also present (see Fig. 11b). It is not yet observed the coarsening process for the Q particles (already observed in Fig. 8a and b for the alloys treated during 6 h), while Mg_2Si is already observed as rounded particles. At this temperature, the quantity of Q surrounding Mg_2Si particles decreased compared to 520 °C. This fact could originate more porosity due to the subsequent shrinkage process, porosity already observed in Figs. 5–7, agreeing with the observed in the DTA studies in Fig. 3 a–c, peaks n. 2, and according to the observed in other works for the transformation of Cu-rich phases at a temperature close to 547 °C [17,20]. A plausible explanation for the more extensive processes

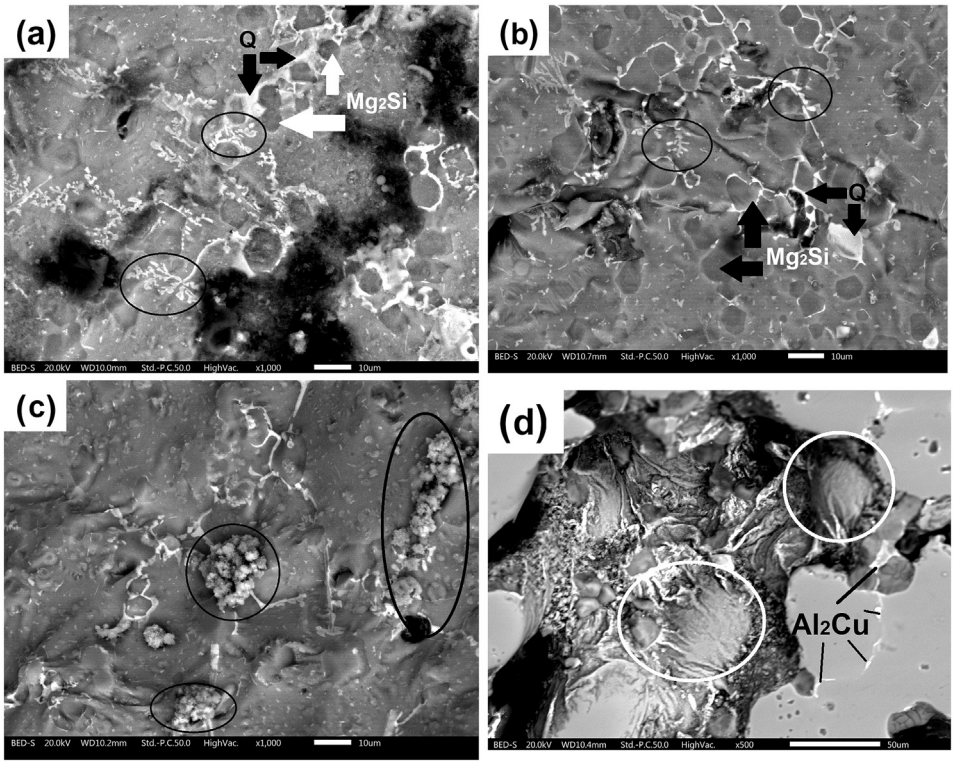

Fig. 11. a, b and c: SEM-BSE micrographs showing the second phases evolution in the alloy with 11% Mg over-solution heat treated during 5 min at temperatures of: (a) 520 °C, (b) 560 °C, and (c) 600 °C. (d) Pore originated in the alloy with 11% Mg over-solution heat treated during 6 h at 600 °C.

for the alloys heat treated at 560 °C, apart from the dissolution effect itself, favored at a higher temperature, could be related to the temperature needed for the reactions already suggested. Finally, at 600 °C the most important result was the presence of irregular agglomerations of several phases (circled in Fig. 11c) with chemical composition also enriched with all the alloying elements. According to this result, it could be thought that at initially, Q and eutectic Mg_2Si phases melted, generating the transformation to the Al_2Cu, Si and primary Mg_2Si phases. This transformation involves not only Cu-rich phases but also eutectic the Al-Mg_2Si phase, agreeing well with that observed using DTA (Fig. 3 a–c, peaks n. 3). This asseveration is also supported by Fig. 11d, which shows a pore originated after a complete heat treatment (600 °C for 6 h). In this image, the pore shows some drops (circled) and is surrounded by the Al_2Cu phase. These results agreed well with the observed in the XRD patters, where for 600 °C the intensity of the Al_2Cu and Si peaks increased; and according to Fig. 8c where Al_2Cu is present close to primary Mg_2Si.

Kinetically, at higher temperature, the atomic diffusion of the low melting point phases is favored; therefore, the heat treatment conducted at 600 °C caused a much higher amount of porosity and modification of the microstructure. It is thought that the high level of porosity obtained at this temperature could be attributed to the much higher amount of liquid phase generated by the melting of Cu-rich phases at 520 and 560 °C, and these phases plus eutectic Mg_2Si when temperature reaches 600 °C. Based on the high amount of possible melted phases, the mechanism proposed by Suarez et al. [6] for the formation of intrinsic highly porous metallic foams, attributed to the large shrinkage generated by peritectic reactions was corroborated. Contrary to binary or tertiary Al alloys, where phases and reactions can be predicted, for quaternary alloys it is very difficult to analyze the evolution of the phases after heat treatments at high temperatures. That is why, and for a deeper analysis of these processes, further works will include the individual characterization in-situ of the phases, heating the alloys at different temperatures. These studies will mainly include in-situ SEM and XRD techniques, in search of a better comprehension not only of the melting process but also the fragmentation, spheroidization and coarsening processes.

3.2.3. Mechanical behavior

Fig. 12 shows the stress (σ) vs. Strain (ε) curves for the foams which contain maxima porosities, obtained using over-solution heat treatments of 600 °C and 6 h. Typical mechanical behavior of compressed foams is barely observed in these curves, attributed to lower porosities when compared to those observed for other metallic foams [1,2]. Bearing in mind that, from the micrographs, the porosity might not be interconnected. Despite of this, for the foam with 40% of porosity (maximum porosity) the curve is similar to the reported by Florek et al. [21] for ductile foams without clear plateau stress or collapse stress. This group of foams exhibits a continuous stress-strain curve without disintegration of material. The three characteristic zones of foamy metallic materials can be clearly identified: Zone I, corresponding to elastic deformation; Zone II (or plateau) where the cell edges are yielding plastically in bending; and Zone III (densification), where the structures compact and stress more significantly rises. Please note that the compression test was carried out with the aim of demonstrating the foamy behavior under compressive strain of the materials investigated. The compliance effect during the test was not subtracted; therefore, the obtained mechanical values are merely illustrative. From these graphs, with the increase in the porosity from 25 to 40% the yield stress decreased from 27.8 MPa to 17.59 MPa; and the compression stress for densification starts also decreased from 55.9 MPa to 36.39 MPa. Besides, as the porosity increases the slope of plateau (Zone II) decreases due to the plastic deformation of the walls and

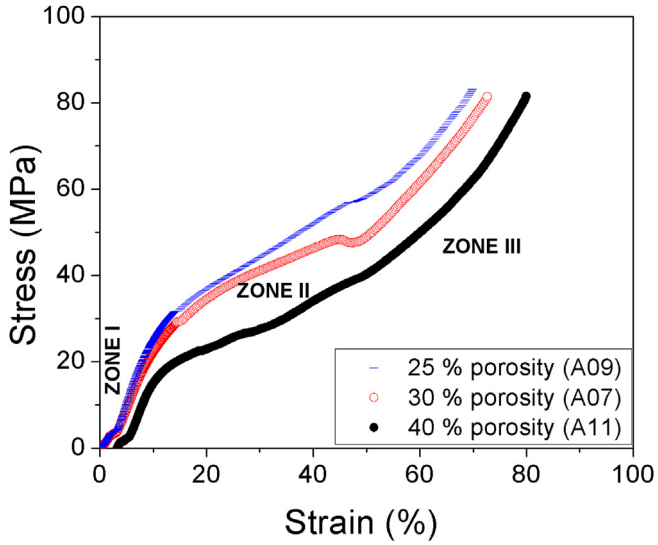

Fig. 12. Compressive stress-strain curves for the foams obtained by over-solution heat treatment of the alloys with Mg contents of 7 wt% (A07), 9 wt% (A09) and 11 wt% (A11), with porosities of 30, 25 and 40%, respectively.

their collapse. So, the lower slope was for the foam with the higher porosity (40%). For the foams with lower porosities (25 and 30%), the mechanical behavior could be cataloged intermediate between foams and solid aluminum alloys due to lower porous concentration. From this, the blocking walls are very large and the mechanical behavior in compression of aluminum predominates. These results agree with the observed by Cadena et al. [22] for foams obtained by powder metallurgy, also decreasing the slope of plateau as the concentration of pores increases, showing the important effect of the porosity on the mechanical behavior of metallic foams [1,2,6]. In summary, in order to decrease the compressive mechanical properties, it is important to increase the amount of porosity. This characteristic can be maximized with over-solution heat treatments of the alloys at the highest possible temperature. Once this point is set, and to obtain a maximum porosity leading to a drop in mechanical properties, the use of an alloy with a high Mg content is desired. Adding this element increases second phases, a necessary condition for obtaining high porosity after their localized melting and transformation. It is important to remark that for these materials the mechanical behavior is not only influenced by the porosity but also by the microstructures with different second phases.

4. Conclusions

After the characterization of the over-solution heat-treated Al-6Si-3Cu-xMg (x = 7, 9 and 11 wt%) alloys, the following conclusions can be written:

1. The effect of the Mg content on microstructure for the as-cast alloys is significant i.e. i) the increment in the Mg content increased the total amount and size of second phases; ii) the predominant second phases for low and high Mg contents were Chinese script Mg_2Si, eutectic Al-Si and Cu-rich phases; iii) for an intermediate Mg content the predominant phases were the Cu-rich ones, besides the primary and eutectic Mg_2Si phases.
2. The porosity amount significantly increased after heat-treating the alloys at 600 °C, reaching a maximum percentage of porosity and pore size of 40% and 150 μm, respectively. Lower heat-treatment temperatures originated low amount porosity. The most rounded shaped pores were obtained for the alloys heat treated at 560 °C.
3. The effect of Mg content on the porosity was not direct but depended on the phases that this element formed. Primary Mg_2Si formation is not desired for obtaining high amount of porosity.
4. Maxima relative densities for the foams obtained using this method are low (between 0.89 and 0.91). Nevertheless, this porosity could contribute increasing the total porosity of the foams obtained using different methods.
5. After the solution heat treatment, the fragmentation, spheroidization and coarsening occurred for Mg_2Si and Q.
6. The most important microstructural modifications after the heat treatments at 520 and 560 °C were for Cu-rich phases and Si, which transformed into Q phase. At 600 °C these phases plus the eutectic Mg_2Si transformed into Al_2Cu, primary Mg_2Si and Si.
7. Pores formation mechanism for these alloys is related mainly to the melted down and dissolution of second phases, followed by large shrinkage generated by the reported reactions.

Acknowledgements

The authors would like to acknowledge the financial support from UNAM PAPIIT IN117316 for funding the project. A. Tejeda and E. H-Mecinas are also acknowledged for they technical support in XRD and compression analyses, respectively.

References

[1] G.J. Davies, S. Zhen, Metallic Foams: their production, properties and applications, J. Mater. Sci. 18 (1983) 1899, http://dx.doi.org/10.1007/BF00554981.
[2] L.J. Gibson, M.F. Ashby, Cellular Solids: Structure and Properties, second ed., Cambridge University Press, Cambridge, 1997.
[3] J. Banhart, Manufacture, characterization and application of cellular metals and metal foams, Prog. Mater. Sci. 46 (2001) 559–632.
[4] M.H. Ismail, R. Goodall, H.A. Davies, I. Todd, Formation of microporous NiTi by transient liquid phase sintering of elemental powders, Mater. Sci. Eng. C 32 (2012) 1480–1485, http://dx.doi.org/10.1016/j.msec.2012.04.02.
[5] I. Alfonso, G. Lara, G. González, L. Béjar, C. Aguilar, I.A. Figueroa, A novel solid state method for manufacturing Al foams by over solution heat treatment, Mater. Lett. 174 (2016) 6–9, http://dx.doi.org/10.1016/j.matlet.2016.03.060.
[6] M.A. Suarez, I.A. Figueroa, G. Gonzalez, G.A. Lara-Rodriguez, O. Novelo-Peralta, I. Alfonso, I.J. Calvo, Production of Al-Cu-Fe metallic foams without foaming agents or space holders, J. Alloy. Compd. 585 (2014) 318–324, http://dx.doi.org/10.1016/j.jallcom.2013.08.015.
[7] F.H. Samuel, A.M. Samuel, P. Ouellet, H.W. Doty, Effect of Mg and Sr additions on the formation of intermetallics in Al-6 Wt pct Si-3.5 Wt pct Cu-(0.45) to (0.8) Wt pct Fe 319-type alloys, Metall. Mater. Trans. A 29 (1998) 2871–2884, http://dx.doi.org/10.1007/s11661-998-0194-y.
[8] I. Alfonso, C. Maldonado, G. Gonzalez, A. Bedolla, Effect of Mg content on the microstructure and dissolution of second phases in Al-Si-Cu-Mg alloys, J. Mater. Sci. 41 (2006) 1945–1952, http://dx.doi.org/10.1007/s10853-006-4494-y.
[9] P. Ouellet, F.H. Samuel, Effect of Mg on the ageing behaviour of Al-Si-Cu 319 type aluminium casting alloys, J. Mater. Sci. 34 (1999) 4671, http://dx.doi.org/10.1023/A:1004645928886Z.
[10] Z. Li, A.M. Samuel, F.H. Samuel, C. Ravindran, S. Valtierra, Effect of alloying elements on the segregation and dissolution of $CuAl_2$ phase in Al-Si-Cu 319 alloys, J. Mater. Sci. 38 (2003) 1203, http://dx.doi.org/10.1023/A:1022857703995.
[11] A.M.A. Mohamed, F.H. Samuel, S. Al Kahtani, Influence of Mg and solution heat treatment on the occurrence of incipient melting in Al–Si–Cu–Mg cast alloys, Mater. Sci. Eng. A 543 (2012) 22–34, http://dx.doi.org/10.1016/j.msea.2012.02.032.
[12] E. Ogris, H. Luchinger, P.J. Uggowitzer, Silicon spheroidization treatment of thixoformed Al-Si-Mg alloys, Mater. Sci. Forum 396–402 (2002) 149–154, http://dx.doi.org/10.4028/www.scientific.net/MSF.396-402.149.
[13] W.S. Rasband, ImageJ, U. S. National Institutes of Health, Bethesda, Maryland, USA, 1997-2015. http://imagej.nih.gov/ij/.
[14] C. Liu, B. Shi, J. Zhou, C. Tang, Quantification and characterization of microporosity by image processing, geometric measurement and statistical methods: application on SEM images of clay materials, Appl. Clay Sci. 54 (2011) 97–106, http://dx.doi.org/10.1016/j.clay.2011.07.022.
[15] D. Yang, Role of Magnesium Addition on the Occurrence of Incipient Melting in Experimental and Commercial Al-si-cu Alloys and its Influence on the Alloy Microstructure and Tensile Properties, Master in Engineering Thesis,

L'université du Québec à Chicoutimi, March 2006.
[16] W. Kasprzak, B.S. Amirkhiz, M. Niewczas, Structure and properties of cast Al–Si based alloy with Zr–V–Ti additions and its evaluation of high temperature performance, J. Alloy. Compd. 595 (2014) 67–79, http://dx.doi.org/10.1016/j.jallcom.2013.11.209.
[17] S. Farahany, N.A. Nordin, A. Ourdjini, T. Abu Bakar, E. Hamzaha, M.H. Idris, A. Hekmat-Ardakan, The sequence of intermetallic formation and solidification pathway of an Al–13Mg–7Si–2Cu in-situ composite, Mater. Charact. 98 (2014) 119–129, http://dx.doi.org/10.1016/j.matchar.2014.09.018.
[18] H. Kezhun, Y. Fuxiao, Z. Dazhi, Z. Liang, Microstructural evolution of direct chill cast Al-15.5Si-4Cu-1Mg-1Ni-0.5Cr alloy during solution treatment, China Foundry 8 (3) (2011) 264–268.
[19] F.H. Samuel, Incipient melting of $Al_5Mg_8Si_6Cu_2$ and Al_2Cu intermetallics in unmodified and strontium-modified Al-Si-Cu-Mg (319) alloys during solution heat treatment, J. Mater. Sci. 33 (1998) 2283–2297, http://dx.doi.org/10.1023/A:1004383203476.
[20] L. Lasa, J.M. Rodriguez-Ibabe, Characterization of the dissolution of the Al2Cu phase in two Al–Si–Cu–Mg casting alloys using calorimetry, Mater. Charact. 48 (2002) 371–378, http://dx.doi.org/10.1016/S1044-5803(02)00283-8.
[21] R. Florek, F. Simančík, M. Nosko, J. Harnúšková, Compression test evaluation method for Aluminium foam parts of different alloys and densities, Powder Metall. Prog. 10 (2010) 207–212.
[22] J.H. Cadena, I.A. Figueroa, M.A. Suarez, O. Novelo-Peralta, G. González, G.A. Lara-Rodríguez, I. Alfonso, Production of Al foams using the SDP method: processing parameters and introduction of a new sintering device, J. Min. Metall. Sect. B-Metall. 52 (1) (2016) 47–52, http://dx.doi.org/10.2298/JMMB150128024C.